A Contact-Adaptive Control Framework for Co-Manipulation Tasks with Application to Collaborative Screwing

Nicola Villa, Emir Mobedi, and Arash Ajoudani

***Abstract*— This paper proposes a novel framework for robotic manipulation tasks, exploiting the Human-Robot Collaboration (HRC) potential. The framework integrates two adaptive controllers to i) modulate robot compliance in contact with the environment along constrained directions, and to ii) enable human guidance through touch when a manual intervention is needed. To demonstrate the potential of the proposed framework, we consider a collaborative screwing task. In this example application, the operator is in charge of placing the screws on the table and following the instructions on a graphical user interface. The robot, after identifying the position of the screws through an online human pose-tracking system, performs the screwing using the proposed controller. The human operator can adjust the screwing position of the robot using the adaptive interface at anytime if the position accuracy through vision is insufficient. We first experimentally evaluate the operation of the proposed controller and demonstrate its performance in comparison to the classical impedance control. Next, the overall system is evaluated in a collaborative (human and robot) setting.**

I. Introduction

Collaborative robots (cobots) are becoming an essential component of smart automation systems in modern industry. The intrinsic characteristics of cobots allow to face the complex challenges that the modern manufacturing poses, such as fast reconfiguration in production lines [1], [2]. The industrial tasks that cobots can address are numerous, most of which can be characterized by the repetition of simple yet effort-demanding sequences. In particular, assembly tasks have a high potential due to their repetitive nature, from which, the most prevalent ones, i.e., screws' fastening and peg-in-hole, constitute 27% and 33% of all the assembly jobs, respectively [3], [4]. In such tasks, however, the uncertainty sources that arise from perception or planning [5] contribute to increasing the complexity of their execution.

The most effective yet low-cost techniques to this problem are based on passive approaches such as the remote center of compliance (RCC) at robot end-effectors, which implement directional adaptation to the uncertainties [6]. Despite their low-cost, it is known that RCC-based and in general, passive solutions cannot respond to the high flexibility needs of today's assembly tasks.

To increase the adaptation capacity of cobots in assembly applications, several interaction control methods including adaptive [7], and hybrid position/force algorithms [8], [9] have been developed. The main idea behind these controllers is to have high stiffness in directions where a high position accuracy is required. In contrast, high compliance can be achieved in the remaining ones, where force adaptation to task constraints is a necessity. In this way, the interaction forces can be regulated by the robot without exerting excessive forces at the task frame. Despite these control strategies, applying a constant force at the end-effector narrows down the potential of robots, since force control is generally employed in a scenario where all the obstacles and possible external effects are well-defined. Indeed, if the contact is lost between the robot and those predefined constraints due to the uncertainties such as human intervention or a small position error, the robot can perform unexpected sudden movements to maintain the desired force at the end-effector. Therefore, serious collisions might arise in the operation area.

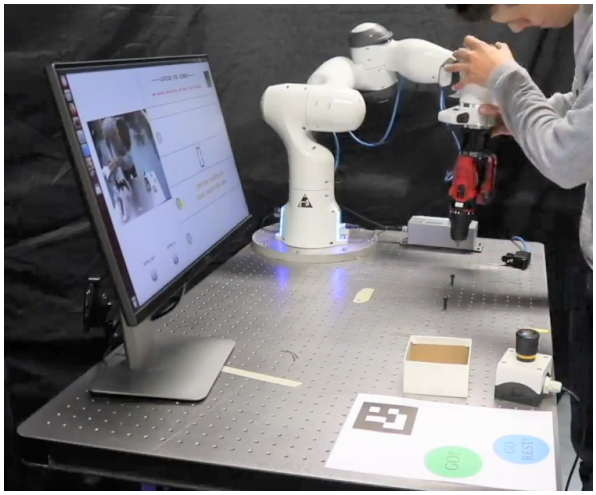

Fig. 1. The proposed control framework aims to improve human-robot collaboration in unstructured manipulation tasks. As an example application, we consider a collaborative screwing task due to its complexity and repetitive nature.

To propose a solution for the above issues, impedance control techniques [5] are developed by programming the robot control gains based on the geometrical constraints of the task frame [10]. However, these gains are usually selected for each particular task by the programmers, which limits the adaptation of robots to various physical interaction scenarios. In addition to the aforementioned model-based methods [7], there are also model-free techniques developed through machine learning algorithms. Mainly, they are classified in two topics as *learn from demonstration* (LfD) and *reinforcement learning* (RL). For the first one, the assembly tasks can be designed to be performed by a human subject whose force and motion data are captured, and transferred to the robot to accomplish the task [11]. Instead, the latter is achieved by

The authors are with the HRI^2 Lab, Istituto Italiano di Tecnologia, Genoa, Italy.

This work was supported by the European Union's Horizon 2020 research and innovation programme under Grant Agreement No. 871237 (SOPHIA)

Manuscript 55 submitted to 2022 31st IEEE International Conference on Robot & Human Interactive Communication (RO-MAN). Received March 11, 2022.

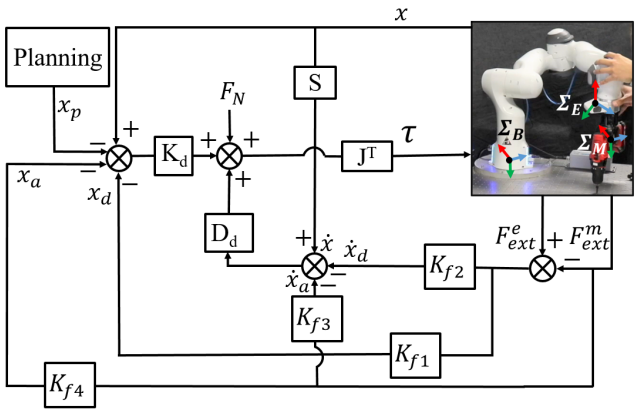

Fig. 2. The block scheme of the contact-adaptive control module.

collecting the data from the environment, where the robot is programmed to execute a particular task in numerous experiments. However, the primary disadvantage of those approaches is to process large experimental data (LfD) or the samples (RL) to verify the adaptation of the robot to different assembly tasks.

Considering the limitations of the current control strategies employed for assembly operations, the aim of this paper is to present a contact-adaptive control framework and validate it within a larger complex manipulation scenario: the collaborative screw fastening (see Fig. 1).

II. Problem Statement

An automated screwing operation can be carried out by a robot in three stages including the detection and an alignment of a screw with the threaded hole, initial thread mating under the clamping force, and finally run-down until the point where the tightening is achieved [12]. During the implementation of the above stages, when the clamping force exceeds the desired level, either the screw or the threaded hole can be damaged. Additionally, if the robot is not programmed to finish the operation when the tightening is accomplished, deformations can be observed in the screw and the threaded hole [13].

To confront these challenges, in the framework presented in this paper, an adaptive control technique is employed [14]. In this controller, the robot stiffness can be modulated in constrained directions depending on the assigned compliance gains and the measured force at the end-effector. In addition, to enable interventions by the operators in case of necessity (e.g., positioning inaccuracies), the adaptive control scheme is applied to two different force information. In more details, a power tool is fixed at the end-effector of the robot and a force sensor is attached on it to measure the interaction forces, while the end-effector forces are estimated through the torque sensors located at the robot joints. The former force data is used to change the robot stiffness depending on the constrained directions (similar to [14]), whereas the latter force information is utilized to adapt the robot trajectories to comply with the operators' needs.

In this collaborative robotic assembly, first, the operator performs the initial thread mating for the screw in a threaded hole which is detected by an external vision system described later in details. Then, a trajectory is planned and commanded to the robot to align with the screw axis. Next, because of the possible position errors of the vision system, the operator moves the robot to perfectly couple the power tool and the screw. After that, a trajectory along the screw axis is commanded to the robot while activating the power tool for screwing operation. By doing this, excessive clamping forces are prevented not to damage the threaded hole or the screw.

Therefore, the implementation of adaptive controller with two different force data enables an autonomous modulation of the robot compliance in constrained directions, while simultaneously improving the collaborative working efficiency of the production system. Hence, human- and task-sourced contacts will be responded differently and appropriately for the benefit of task execution efficiency.

The rest of the paper is organised as follows. Section III explains the framework modules in details. In section IV, the experimental setup is introduced. In section V, the experimental results are discussed. Finally, conclusion and the future studies are discussed in section VI.

III. The Collaborative Robotic Assembly Framework

This section describes the proposed contact-adaptive controller within a larger collaborative framework for industrial screwing tasks, which also includes additional modules such as a vision system for screws detection, a Graphical User Interface (GUI) for human-robot communication, and an interaction planner for managing the transitions.

A. Contact-adaptive controller module

In Fig.2, the block scheme of the contact-adaptive control framework is presented. The generalised coordinates are denoted as $\boldsymbol{q} \in \mathbb{R}^n$, and the dynamic equation of motion for n-DoFs robot can be written as:

$$\boldsymbol{M}(\boldsymbol{q})\ddot{\boldsymbol{q}} + \boldsymbol{C}(\boldsymbol{q},\dot{\boldsymbol{q}})\dot{\boldsymbol{q}} + \boldsymbol{g}(\boldsymbol{q}) = \boldsymbol{\tau} + \boldsymbol{\tau}_{ext}, \tag{1}$$

where $\boldsymbol{M}(\boldsymbol{q})$ is the $n \times n$ inertia matrix, $\boldsymbol{C}(\boldsymbol{q},\dot{\boldsymbol{q}})$ is the Coriolis/centrifugal matrix, $\boldsymbol{g}(\boldsymbol{q})$ is the vector of gravity joints torques, and $\boldsymbol{\tau}$ is the vector of actuated joint torques. $\boldsymbol{\tau}_{ext} = \boldsymbol{J}(\boldsymbol{q})^T \boldsymbol{F}_{ext}$ represents the reaction torques that are used by the k linearly independent constraint forces $\boldsymbol{F}_{ext} \in \mathbb{R}^k$ and the Jacobian matrix $\boldsymbol{J}(\boldsymbol{q}) \in \mathbb{R}^{k\times n}$. To clarify, $\boldsymbol{F}_{ext}$ is a external wrench at the robot's end-effector in Cartesian space (i.e. k = 6).

Therefore, the dynamic behavior in Cartesian space can be examined as:

$$\boldsymbol{\Lambda}_d\ddot{\tilde{\boldsymbol{x}}} + \boldsymbol{D}_d\dot{\tilde{\boldsymbol{x}}} + \boldsymbol{K}_d\tilde{\boldsymbol{x}} = \boldsymbol{F}_{ext}, \tag{2}$$

where $\tilde{\boldsymbol{x}} = \boldsymbol{x} - \boldsymbol{x}_d \in \mathbb{R}^6$ represents the Cartesian error calculated with respect to the desired Cartesian coordinates $\boldsymbol{x}_d$. Also, $\boldsymbol{\Lambda}_d$, $\boldsymbol{D}_d$ and $\boldsymbol{K}_d$ are desired Cartesian ($\in \mathbb{R}^{6\times6}$) inertia, damping and stiffness matrices (positive definite and symmetric) respectively. If the inertia shaping is neglected and the desired velocity is considered to be zero, (2) can be simplified to:

Manuscript 55 submitted to 2022 31st IEEE International Conference on Robot & Human Interactive Communication (RO-MAN). Received March 11, 2022.

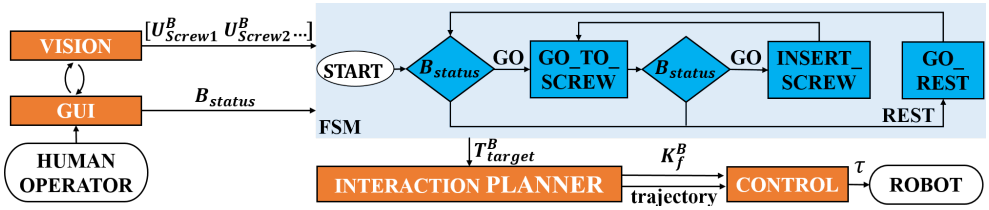

Fig. 3. The Finite State Machine and the Modules communication chart, where $\boldsymbol{T}^B_{target} \in \{\boldsymbol{T}^B_{screw}, \boldsymbol{T}^B_{insert}, \boldsymbol{T}^B_{rest}\}$ and $\boldsymbol{B_{status}} \in$ {GO,REST}.

$$\boldsymbol{D}_d\dot{\tilde{\boldsymbol{x}}} + \boldsymbol{K}_d\tilde{\boldsymbol{x}} = \boldsymbol{F}_{ext}. \tag{3}$$

As $\boldsymbol{K}_d$ and $\boldsymbol{D}_d$ are the impedance control gains that have to be adjusted properly depending on the specific geometrical task constraints, they limit the robot capability to cope with uncertainties such as mismatches between screw and the robot. To enhance the adaptation of the robot to the targeted co-assembly task, the modification is done in (3), and the desired dynamic behavior for the contact-adaptive controller in Cartesian space is defined as:

$$\boldsymbol{D}_d(\dot{\boldsymbol{x}} - \dot{\boldsymbol{x}_C}) + \boldsymbol{K}_d(\boldsymbol{x} - \boldsymbol{x}_C) = \boldsymbol{F}_{ext}, \tag{4}$$

where,

$$\boldsymbol{x}_C = \boldsymbol{x}_d + \boldsymbol{x}_P + \boldsymbol{x}_a, \tag{5}$$

and

$$\dot{\boldsymbol{x}_C} = \dot{\boldsymbol{x}_d} + \dot{\boldsymbol{x}_P} + \dot{\boldsymbol{x}_a}. \tag{6}$$

Regarding the adaptive controller, the following equations are used:

$$\boldsymbol{x}_d = \boldsymbol{K}_{f1}(\overbrace{\boldsymbol{F}^e_{ext} - \boldsymbol{F}^m_{ext}}^{\boldsymbol{F}_{Human}}) \qquad \dot{\boldsymbol{x}}_d = \boldsymbol{K}_{f2}(\overbrace{\boldsymbol{F}^e_{ext} - \boldsymbol{F}^m_{ext}}^{\boldsymbol{F}_{Human}}), \tag{7}$$

and

$$\boldsymbol{x}_a = \boldsymbol{K}_{f4}\boldsymbol{F}_{ext} \qquad \dot{\boldsymbol{x}}_a = \boldsymbol{K}_{f3}\boldsymbol{F}_{ext}. \tag{8}$$

$\boldsymbol{K}_{f1}$, $\boldsymbol{K}_{f2}$ ($\in \mathbb{R}^{6\times6}$) are the inverse damping and stiffness matrices (diagonal and positive definite) respectively. Similarly, $\boldsymbol{K}_{f3}$, and $\boldsymbol{K}_{f4}$ are used for both inverse damping and stiffness (compliance matrix) in (8). Additionally, $\boldsymbol{x_P}$ is the desired trajectory, and $\dot{\boldsymbol{x}}_P$ is the desired velocity that is considered as zero in (6).

As mentioned before, two force information are considered as $\boldsymbol{F}^m_{ext}$, and $\boldsymbol{F}^e_{ext}$. The former one is acquired through a F/T sensor in the tool frame (Σ_M in Fig. 2), which is attached to the power tool. Instead, the latter is estimated in end-effector frame (Σ_E) through a formulation presented in [15]. The reason to measure two different forces is to separate the physical interactions in Σ_E (between human and the robot), and in Σ_M (between the tool and the screw).

It is important to note that $\boldsymbol{F}^m_{ext}$ is transformed to Σ_E, and then subtracted from $\boldsymbol{F}^e_{ext}$ in the calculation of the applied human force. Afterwards, all the resultant force components are resolved in Σ_B.

According to the working principle of the contact-adaptive controller, if the robot is commanded a trajectory ($\boldsymbol{x}_P$) in free space without physical interaction ($\boldsymbol{F}^m_{ext} = \boldsymbol{F}^e_{ext} = 0$), $\boldsymbol{x}_d$ and $\boldsymbol{x}_a$ terms become zero. Therefore, the proposed controller works as the cartesian impedance controller, and the robot follows the trajectory depending on the assigned $\boldsymbol{K}_d$ and $\boldsymbol{D}_d$ control gains. Additionally, when the physical interaction between human and the robot occurs only in Σ_E without commanding a trajectory, $\boldsymbol{x}_P$ and $\boldsymbol{x}_a$ become zero. Hence, the trajectory of the robot ($\boldsymbol{x}_d$) is calculated depending on the applied human force, $\boldsymbol{K}_{f1}$, $\boldsymbol{K}_{f2}$ and impedance control gains. Important to note that these calculated $\boldsymbol{x}_d$ values are integrated during the physical interaction, and sent to the robot as the desired trajectory. Therefore, the robot keeps its last position even if the physical interaction is lost. This is the main novelty of the proposed controller that allows us to change the robot position with the help of a human.

Furthermore, when the physical interaction emerges in Σ_M while a human is moving the robot from Σ_E, the trajectory of the robot is changed through $\boldsymbol{x}_d$ term. Meanwhile, $\boldsymbol{x}_a$, and $\dot{\boldsymbol{x}}_a$ terms are also calculated depending on the assigned $\boldsymbol{K}_{f3}$, and $\boldsymbol{K}_{f4}$ gains to regulate the robot force response in Σ_M. As an example application of the contact-adaptive controller, the implementation of the collaborative screwing assembly is explained that includes the above mentioned interaction scenarios between the operator, the robot, and the environment.

First, a predefined trajectory ($\boldsymbol{x}_P$) is commanded to the robot to align with the screw axis. During this interval, there is no physical interaction in neither Σ_M nor Σ_E and the robot is governed by the Cartesian impedance controller. Afterwards, the operator moves the robot ($\boldsymbol{x}_d$) to be perfectly aligned with the power tool, and to mate the screw and the Allen key attached on the power tool. Finally, the robot executes a trajectory along the screw axis to apply clamping force, and the power tool is activated to complete the screwing operation. In the course of this period, the adaptive controller ($\boldsymbol{x}_a$) implements a compliant force profile along the screw axis, and stiff in all other directions. By doing this, excessive clamping forces are prevented not to damage the teethes of threaded hole or the screw.

B. Vision Module and GUI

This chapter explains the vision module, and the graphical user interface (GUI) that are developed to detect the position of the screw with respect to the Σ_B (see Fig.2), and to guide the human operator to achieve the collaborative assembly. To start with, the human operator performs the initial thread mating between the screw and the threaded hole on a table.

Then, the operator is asked to wait three seconds while holding the screw. During this interval, the position of the screw is identified from the estimated 3D human skeleton points using the online OpenPose algorithm [16]. Next, the GUI gives visual feedback stating that the hand of the user can be removed from the screw.

After that step, a camera detects the normal axis (z) of the screw through the 3D point cloud method. Hence, the new frame (Σ_S) is defined on top of the screw assigning the other axes (y and x) arbitrarily to create a cartesian triad.

Moreover, the operator can send commands to the developed control framework via a virtual button board. This consists of colored markers placed on the test experiment area (see Fig.4). The user can press the desired button by keeping the hand fixed on the relative marker. Then, the algorithm receives feedback from OpenPose hand detection and ensures that the hand is fixed on a specific marker. Therefore, the button is considered as pressed in the control loop, and the GUI gives visual feedback to the human operator as "BUTTON_GO". A similar strategy is employed for the other button defined as "BUTTON_REST".

C. Interaction planner module

The goal of the interaction planning module is to generate a 5^{th} order polynomial trajectory to roughly align the drilling machine with the screw pose. To do that, a transformation matrix is composed as $\boldsymbol{T}^B_{target}$ from Σ_B to target frames such as $\boldsymbol{T}^B_{screw}$ and $\boldsymbol{T}^B_{rest}$ that will be explained in detail in the next module. Additionally, this module regulates the robot stiffness to be more compliant along the screw normal axis than the rest of the DoFs. This is achieved by assigning K_f gain above zero along the screw axis in the adaptive control. Instead, for the other cartesian axes, zero K_f are selected to have high tracking capability.

Since the human operator performs the initial mating between the drilling machine and the screw, they are always aligned in the same z axis. Hence, $\boldsymbol{K}_f$ matrix is defined in Σ_M, and represented as $\boldsymbol{K}^M_f$. However, as all the calculations are implemented in Σ_B in (4), $\boldsymbol{K}_f$ is transformed from Σ_M to Σ_B with the help of $\boldsymbol{R}^B_M$ transformation matrix.

Therefore, $\boldsymbol{K}^B_f$ is computed using $\mathfrak{R}\,\boldsymbol{K}^D_f\,\mathfrak{R}^T$, which denotes the Singular Value Decomposition of the $\boldsymbol{K}^B_f$. $\mathfrak{R}$ is:

$$\mathfrak{R} = \begin{bmatrix} \boldsymbol{R}^B_D & \mathbf{0}_{3\times3} \\ \mathbf{0}_{3\times3} & \boldsymbol{R}^B_D \end{bmatrix}, \tag{9}$$

D. Finite State Machine (FSM)

The communication between the abovementioned modules is performed through a FSM. The unified control framework is illustrated in Fig.3, and developed to achieve several screwing operation. However, the control framework is explained for the assembly of two screws here to verify the method.

First, the vision module sends the detected screws (i.e. $\boldsymbol{U}^B_{Screw1}$, $\boldsymbol{U}^B_{Screw2}$,...) to the FSM. This has 3 states: *go_to_screw* (S1), *insert_screw* (S2), *go_rest* (S3). The interaction planner module receives $\boldsymbol{T}^B_{target}$ by the FSM and

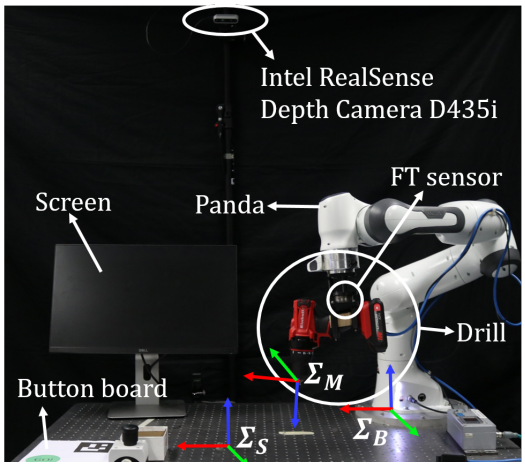

Fig. 4. Illustration of the experimental setup.

sends the computed trajectory and $\boldsymbol{K}^B_f$ to the controller. $\boldsymbol{T}^B_{target}$ is a transformation matrix from Σ_B to a target pose, which is different for each state: $\boldsymbol{T}^B_{screw}$ (top of the screw) for S1, $\boldsymbol{T}^B_{insert}$ (bottom of the screw) for S2 and $\boldsymbol{T}^B_{rest}$ for S3.

To start with, when $\boldsymbol{B}_{status}$ is "GO" (BUTTON_GO), the robot follows the planned trajectory, and goes towards to the first screw. When it reaches roughly the screw position, the human operator couples the drilling machine with the screw. Next, the human operator presses again BUTTON_GO ($\boldsymbol{B}_{status} = GO$), and the robot starts to go forward along the screw normal axis. During this interval, the drilling machine is also activated to rotate the screw. When the screw is inserted, the FSM triggers S1 for processing the next screw in the queue. Then, the worker presses again BUTTON_GO ($\boldsymbol{B}_{status} = GO$) and the similar task sequence mentioned above is repeated to achieve the assembly.

Important to note that, if the user presses BUTTON_REST ($\boldsymbol{B}_{status} = REST$) in any states due to an unexpected problem, the robot executes S3 state moving back to a predefined rest pose.

IV. Experimental Setup

The experimental setup and reference frames are illustrated in Fig.4. A Franka Emika Panda arm, whose end-effector was coupled with a F/T sensor (ATI-Mini45, SI 145-5) is used for the proposed framework. In addition, an electrical drill ($1.3kg$) was attached to F/T sensor. A camera (Intel RealSense Depth Camera D435i) is mounted on a fixed apparatus for the detection of the screw. Additionally, M6 hex screws are used to assemble them on a metal table where a number of threaded holes are opened. It is important to note that all the calculations including $\boldsymbol{F}^e_{ext}$ and $\boldsymbol{F}^m_{ext}$ are carried out in $\boldsymbol{\Sigma}_B$.

Regarding the control gain selection, there are 6 matrices in (4): $\boldsymbol{K}_d$, $\boldsymbol{D}_d$, $\boldsymbol{K}_{f1}$, $\boldsymbol{K}_{f2}$, $\boldsymbol{K}_{f3}$, and $\boldsymbol{K}_{f4}$. The first two are set high to guarantee a good tracking capability, as in [14]. When it comes to $\boldsymbol{K}_{f3}$ and $\boldsymbol{K}_{f4}$, they are selected equal to each other and denoted as $\boldsymbol{K}_f$ from now on. To have adaptive behavior in z axis, only K_{fz} is selected above

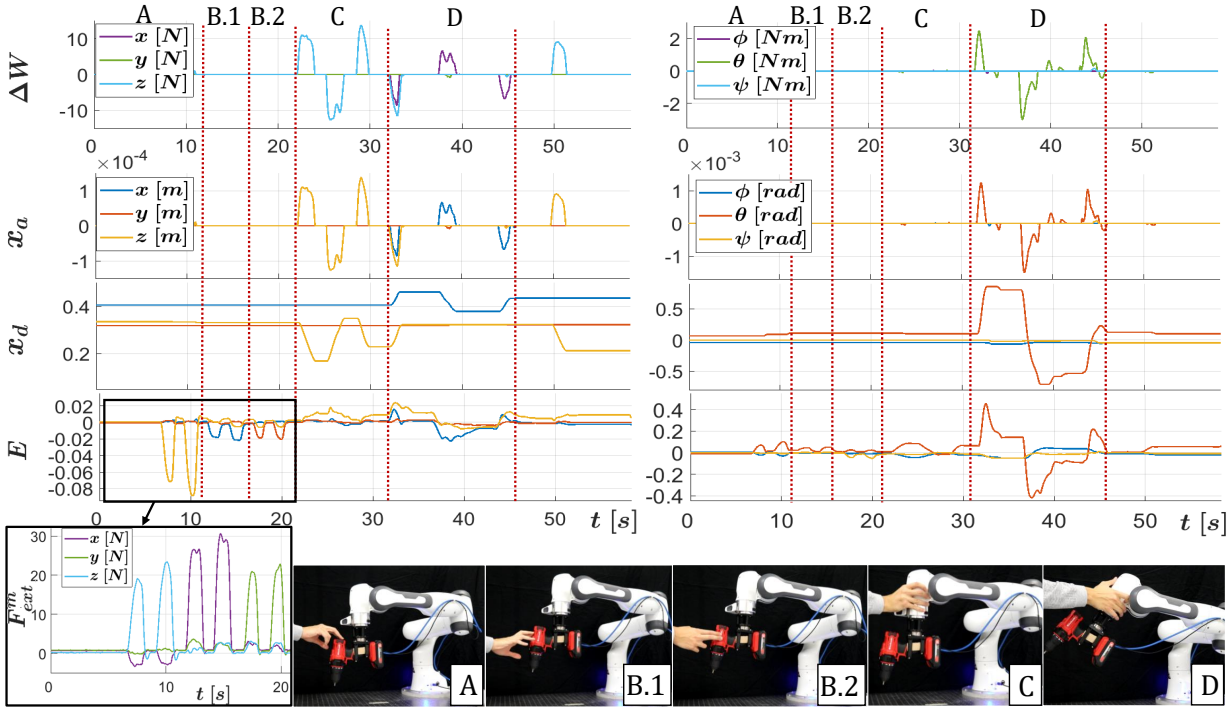

Fig. 5. The experimental results of the controller validation test.

zero to achieve a soft interaction between the screw aligned by a human operator and the robot. Instead, all the other directions are assigned as 0 to have high position accuracy.

For $\boldsymbol{K}_{f1}$ and $\boldsymbol{K}_{f2}$, the selection of higher gains lead to have smaller position variation ($\boldsymbol{x}_d$), which means to perform sensitive behaviour. Hence, they are selected experimentally to provide a comfortable yet steady way to move the robot.

In the assembly scenario, when the power tool contacts with the screw, the interaction forces are decreased along z axis according to (8). Nevertheless, since the power tool turns the screw, and it starts to enter the hole, this causes the reduction of contact force ($\boldsymbol{F}^m_{ext}$) between the power tool and the screw. The lower force generates lower $\boldsymbol{x}_a$ and $\dot{\boldsymbol{x}}_a$ terms in (8), and the manipulator starts to push against the screw while keeping the contact. This dynamic continues until the screw is completely inserted. It is clear how this approach eventually guarantees that the minimum force required to maintain the contact is applied on the screw, both during the process and at the end of the stroke, in case the screw length is not exactly known.

In this work, $\boldsymbol{K}_d$ has fixed-high values as $K_{dx} = K_{dy} = K_{dz} = 1000\,\mathrm{m/N}$ and $K_{droll} = K_{dpitch} = K_{dyaw} = 30\,\mathrm{rad/Nm}$. Regarding the adaptive impedance controller, the diagonal compliance matrix gains are assigned as $K_{fx} = K_{fy} = 0\,\mathrm{m/N}$, and for the orientations $K_{froll} = K_{fpitch} = K_{fyaw} = 0\,\mathrm{rad/Nm}$. $K_{fz} = 0.003$ m/N enables to have a stiff behavior in insertion direction (z).

In addition, $K_{f1x} = K_{f1y} = K_{f1z} = 100000\,\mathrm{m/N}$, $K_{f1roll} = K_{f1pitch} = K_{f1yaw} = 2000\,\mathrm{rad/Nm}$, $K_{f2x} = K_{f2y} = K_{f2z} = 5000\,\mathrm{m/N}$; and $K_{f2roll} = K_{f2pitch} = K_{f2yaw} = 200\,\mathrm{rad/Nm}$. The behaviour of the controller, hence the reasons to choose these parameters, are explain in the following.

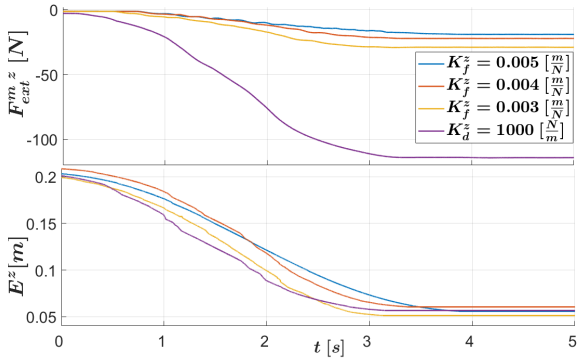

Fig. 6. The comparison of interaction forces and E^z term for impedance and contact-adaptive controllers during the S2 phase (*insert_screw*).

V. Experimental Results

A. Controller Verification

The aim of this experiment is to validate the working principle of the proposed contact-adaptive controller. This is carried out by the human operator moving the power tool arbitrarily in certain directions. The linear ($\boldsymbol{x}$, $\boldsymbol{y}$, $\boldsymbol{z}$) and angular (roll ($\boldsymbol{\phi}$), pitch ($\boldsymbol{\theta}$) and yaw ($\boldsymbol{\psi}$)) position variations of the robot are illustrated on the left and right of the Fig.5, respectively. Additionally, $\boldsymbol{\Delta W}$ corresponds to $\boldsymbol{F}_{Human}$ in (7), and $\boldsymbol{E}$ denotes the difference between $\boldsymbol{x}_d$ and $\boldsymbol{x}_a$.

First, the robot is located at the initial position (without any contact) that can be observed from $\boldsymbol{x}_d$ data in Fig.5. In

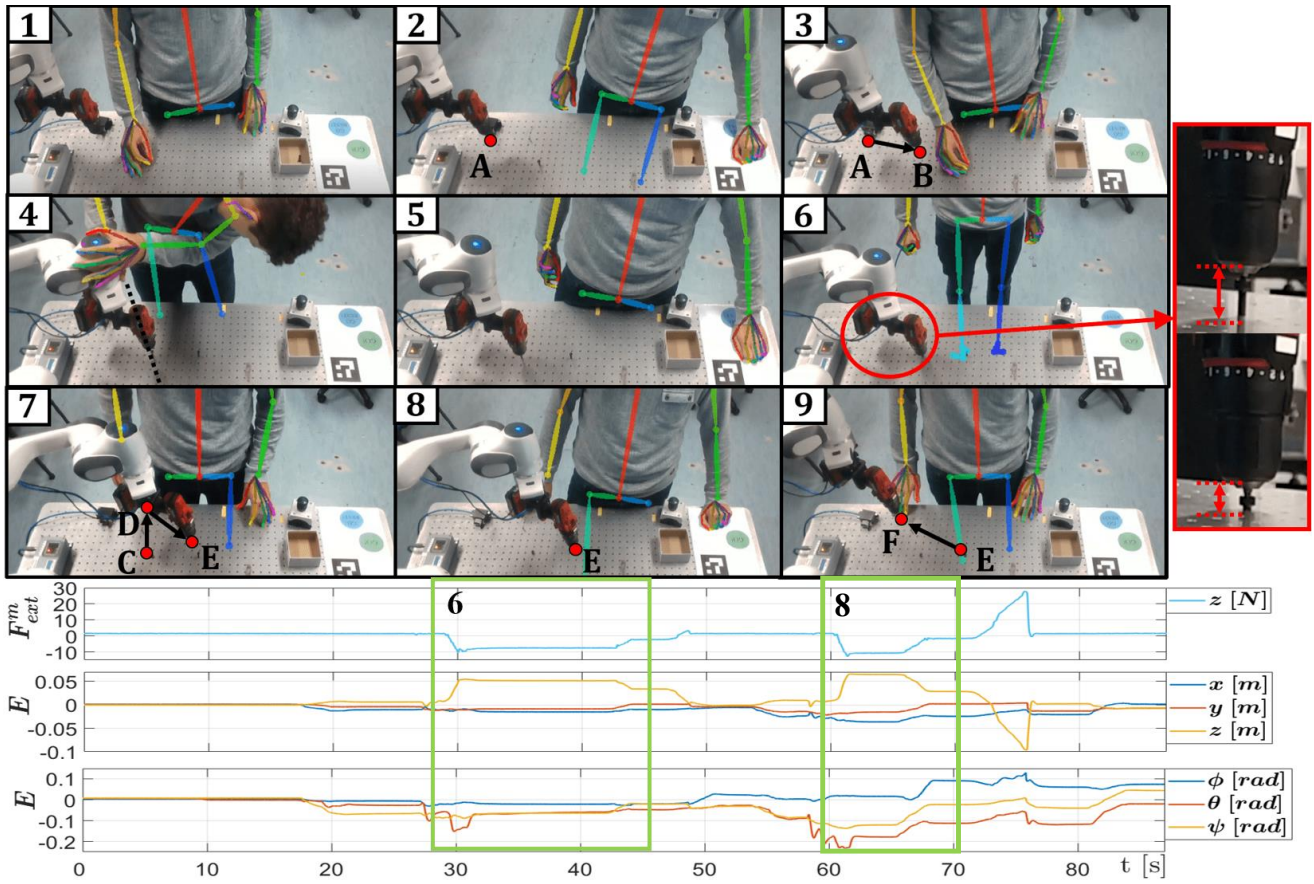

Fig. 7. The experimental results for framework validation: snapshots for illustrating the collaborative screwing assembly (on top), and the variation of interaction forces ($\boldsymbol{F}^m_{ext}$) along z axis, and E terms for all Dofs.

the first three phases (A, B.1, and B.2), the operator exerts a force on the power tool, and this leads to having equal $\boldsymbol{F}^m_{ext}$ and $\boldsymbol{F}^e_{ext}$. Hence, $\boldsymbol{\Delta W}$ becomes zero, and $\boldsymbol{x_d}$ is not updated according to (7). Only $\boldsymbol{x_a}$ term has an effect on the robot, and this can be easily monitored from $\boldsymbol{E}$ graph displaying a non-zero position trend. Specifically, as K_{fz} is greater than K_{fx}, and K_{fy}, the robot has stiffer behavior along x and y axes than z. This can be also clearly seen from the multimedia attachment.

In C and D phases, the operator moves the robot along z axis and pitch orientation from Σ_E. In this case, since $\boldsymbol{\Delta W}$ is different than zero, $\boldsymbol{x}_d$ is varied depending on the applied human force, and the assigned $\boldsymbol{K}_{f1}$ and $\boldsymbol{K}_{f2}$ compliance gains.

Afterward, the proposed contact-adaptive controller is compared with the impedance controller in terms of interaction forces in Σ_M employing the second phase of the assembly (*insert_screw* (S2)). First, the power tool is coupled with the screw, and the robot is moved 15 cm along z axis while activating the power tool for screwing. This task is repeated using different K_{fz} values to demonstrate the variation of the interaction forces (see Fig. 6).

Finally, the same trial is performed with an impedance controller assigning stiff K_{dz}. The results show that the interaction forces are sharply higher for impedance control ($\approx$ 110 N) than the proposed controller ($\approx$ 20 N).

B. Framework Validation

In this experiment, the whole framework is implemented, and the experiment's flow is illustrated in Fig.7. In step-1, the human operator performs the initial thread mating between the screw and the table. Then, the operator waits three seconds following GUI feedback for the detection of the screw pose. In step-2, the user presses BUTTON_GO, and the robot goes towards the screw. In the next step, the operator places a second screw on the table as in step-1. In step-4, the operator couples the power tool and the screw manually, pressing BUTTON_GO to start the screwing operation (step-5 and 6). The detailed view of the screw length variation is illustrated in the red box (on the left part of the Fig.7).

In step-7, the robot goes towards the second screw following C-D and D-E points. During this interval, since there is no physical interaction, $\boldsymbol{F}^m_{ext}$ and $\boldsymbol{E}$ values become zero. Hence, the robot is controlled by the impedance controller.

It is clear that when the contact occurs between the screw and the power tool (step-6 and 8), $\boldsymbol{E}$ graph changes depending on the sensed force direction (highlighted with green box). Additionally, resultant interaction forces ($\boldsymbol{F}^m_{ext}$) and $\boldsymbol{E}$ values display similar curves in step-6 and 8, verifying

Manuscript 55 submitted to 2022 31st IEEE International Conference on Robot & Human Interactive Communication (RO-MAN). Received March 11, 2022.

the repeatability of the controller for multi-screwing task.

VI. Conclusion

In this work, we proposed a novel HRC framework for robotic screwing. This is composed of an adaptive controller acting on two force information, a vision system, a GUI, an interaction planner and a FSM. The controller was first tested to show its operation. Then, it was compared with an impedance control to show the strength of the proposed strategy. Next, the integrated framework was evaluated in a collaborative multi-screwing task. The operator could intervene in the process when necessary, while the controller effectively modulated the force on the screw. Results revealed the high potential of the approach in successful execution of industrial screwing tasks.

References

[1] A. Ajoudani, A. M. Zanchettin, S. Ivaldi, A. Albu-Schäffer, K. Kosuge, and O. Khatib, "Progress and prospects of the human–robot collaboration," *Autonomous Robots*, vol. 42, no. 5, pp. 957–975, 2018.

[2] D. Küpper, M. Lorenz, C. Knizek, K. Kuhlmann, A. Maue, R. Lässig, and T. Buchner, "Advanced robotics in the factory of the future," *Boston Consulting Group*, March 2019.

[3] E. J. Nicolson, *Grasp stiffness solutions for threaded insertion*. University of California, Berkeley, 1990.

[4] J. L. Nevins and D. E. Whitney, "Computer-controlled assembly," *Scientific American*, vol. 238, no. 2, pp. 62–75, 1978.

[5] R. Ahmad and P. Plapper, "Safe and automated assembly process using vision assisted robot manipulator," *Procedia CIRP*, vol. 41, pp. 771 – 776, 2016.

[6] N. Ciblak and H. Lipkin, "Design and analysis of remote center of compliance structures," *J. Field Robotics*, vol. 20, pp. 415–427, 2003.

[7] J. Xu, Z. Hou, Z. Liu, and H. Qiao, "Compare contact model-based control and contact model-free learning: A survey of robotic peg-in-hole assembly strategies," 04 2019.

[8] H. Abdullah, Mustafa W.and Roth, M. Weyrich, and J. Wahrburg, "An approach for peg-in-hole assembling using intuitive search algorithm based on human behavior and carried by sensors guided industrial robot," *International Federation of Automatic Control*, vol. 48, pp. 1476–1481, 2015.

[9] H. Park, J. Park, D.-H. Lee, J.-H. Park, M.-H. Baeg, and J.-H. Bae, "Compliance-based robotic peg-in-hole assembly strategy without force feedback," *IEEE Transactions on Industrial Electronics*, vol. 64, pp. 6299–6309, 2017.

[10] A. Ajoudani, N. Tsagarakis, and A. Bicchi, "Tele-impedance: Teleoperation with impedance regulation using a body–machine interface," *The International Journal of Robotics Research*, vol. 31, no. 13, pp. 1642–1656, 2012.

[11] B. Argall, S. Chernova, M. Veloso, and B. Browning, "A survey of robot learning from demonstration," pp. 469–483, 09 2017.

[12] Z. Jia, A. Bhatia, R. M. Aronson, D. Bourne, and M. T. Mason, "A survey of automated threaded fastening," *IEEE Transactions on Automation Science and Engineering*, vol. 16, no. 1, pp. 298–310, 2019.

[13] X. Xiaohui, G. Li, F. Zhang, and L. Sun, *A Force Control Robot Screwing System Design for Plastic Workpiece: Proceedings of International Conference on Mechatronics and Intelligent Robotics (ICMIR2018)*, 2019, pp. 603–609.

[14] E. Mobedi, N. Villa, W. Kim, and A. Ajoudani, "An adaptive control approach to robotic assembly with uncertainties in vision and dynamics," in *IEEE International Conference on Robot and Human Interactive Communication*. IEEE, 2020.

[15] A. D. Luca, A. Albu-Schaffer, S. Haddadin, and G. Hirzinger, "Collision detection and safe reaction with the DLR-III lightweight manipulator arm," pp. 1623–1630, 2006.

[16] Z. Cao, G. Hidalgo Martinez, T. Simon, S. Wei, and Y. A. Sheikh, "Openpose: Realtime multi-person 2d pose estimation using part affinity fields," *IEEE Transactions on Pattern Analysis and Machine Intelligence*, 2019.